PAPER

Check for updates

Aquaporin embedded suspended lipid bilayer on anodized alumina nanoporous substrates for studying stability and functionality: towards the development of a miniaturized water purifier

Akanksha Kumari,[a] Jaydeep Bhattacharya ✱[b] and Ranjita Ghosh Moulick ✱[a]

Porous substrates are crucial for suspended lipid bilayers, yet the influence of pore dimensions on bilayer stability and function remains underexplored. Understanding how these complementary platforms affect bilayer properties is essential for developing reliable biomimetic systems, and studying transmembrane proteins. We fabricated pores at different scales (micro- and nanoscale) by employing an aluminium-based substrate, using manual puncturing for micropores and anodization for nanopores. This approach was designed to address the intricate role of porous substrates in modulating the bilayer suspension, stability and function of 1-palmitoyl-2-oleoyl-*glycero*-3-phosphocholine (POPC) lipid bilayers. Micropores provide optical access for real-time imaging of bilayer coverage and defects, while nanopores offer stronger mechanical stability, as confirmed by impedance spectroscopy with giga-seal resistance (∼2 GΩ). Using this stable platform, aquaporin, a water-channel protein, was reconstituted into lipid bilayers using an *n*-octyl-β-ᴅ glucopyranoside (NOG) detergent-mediated method. Dynamic light scattering, zeta potential, and impedance analyses confirmed successful insertion, and forward osmosis assays demonstrated functional water transport. The study represents a comparative framework, demonstrating the trade-off between accessibility and stability and providing design principles for future bilayer-based biomimetic and protein reconstitution platforms.

Introduction

Membrane models composed solely of lipids or lipid mixtures are invaluable platforms for investigating membrane biophysics.[1,2] These biomimetic systems, while significantly reduced in complexity compared to living membranes, offer precise experimental control and enable detailed structural analyses of membrane behaviour and interactions.[3] For example, planar lipid bilayers on substrates like glass or mica have been widely used to study protein–lipid interactions, membrane biophysics, biosensing, and drug discovery.[4–6] Lipid bilayers on solid substrates are a common and efficient method of artificial bilayer formation, except in applications that require bilateral access within the lipid bilayer. The lack of spacing between the bilayer and the substrate hinders the integration of channel proteins (like aquaporins) into the system.[7,8] Consequently, pore-spanning or suspended lipid bilayer systems have been developed, which hang on the air–water interface, rather than resting on any physical substrate.

This provides a suitable platform to investigate mechanisms of molecular transport and protein functionality.[9,10]

However, it is difficult to achieve stability in lipid bilayers suspended over porous substrates. These bilayers are highly susceptible to rupture due to physical and chemical stresses, including mechanical forces, osmotic imbalances, and thermal fluctuations.[11,12] The pore geometry of the supporting substrate plays a decisive role in bilayer stability and function.[8,11] Porosity impacts applications ranging from DNA separation using anodic alumina (AAO) filters to drug delivery and biointerfaces with proteins and peptides.[3,8,12–14] While previous studies have demonstrated bilayer formation on porous substrates, there is limited systematic understanding of how the pore scale, from micro to nano, modulates stability, lipid mobility, and protein functionality in the same experimental framework. Thus, investigating suspended lipid bilayers across different pore scales (micro-, meso-, and nano-) offers unique advantages and trade-offs. The characterization of such systems differs fundamentally from those used for liposomes or supported lipid bilayers. Fluorescence microscopy is indispensable for studying suspended bilayers because it enables direct visualization of bilayer coverage, defects, and structural continuity, features that electrochemical impedance spectroscopy alone cannot resolve. Although EIS can detect changes in global membrane resistance and defect density, it cannot image local discontinuities or spatial heterogeneity that microscopy readily

[a]Amity Institute of Biotechnology, Amity University Haryana, 122413, India. E-mail: ranjita.ghoshmoulick@gmail.com

[b]School of Biotechnology, Jawaharlal Nehru University, New Delhi, 110067, India. E-mail: jaydpb@gmail.com

captures. Micropores, due to their larger size, afford optical access and allow researchers to observe bilayer distribution in real-time directly under the microscope. In contrast, nanopores offer greater mechanical stability, making them well-suited for long-term electrochemical measurements and functional testing (*e.g.*, protein reconstitution). Thus, different applications demand porous substrates of different dimensions depending on whether the priority is optical characterization or robust electrical/functional performance.[11,15,16]

Understanding the importance of structural parameters of substrates in advancing platforms for suspended lipid bilayers, and focusing on strategies to overcome related limitations, is essential for advancing membrane biophysics. These parameters directly dictate bilayer lifetime, mechanical stability, and compatibility with functional assays, that ultimately determine whether such systems can transition from basic biophysical models to reliable platforms for biosensing, membrane protein analysis, and biomimetic filtration.

Our approach combines direct experimental comparison of micro-*versus* nanopores with functional validation using a model water-channel protein, aquaporin.[16,17] Aquaporin-based water purification systems represent a potential biomimetic approach due to their exceptionally high-water permeability and selectivity, closely mimicking natural water channels. This study enables us to identify how pore architecture governs membrane stability, lipid mobility, and protein activity, providing mechanistic insights that have been underexplored, bridging optical and electrochemical characterization across two pore scales within the same framework. Furthermore, understanding and optimizing these factors can enable the development of portable, cost-effective, and reliable water purification units.

Experimental

Materials

1-Palmitoyl-2-oleoyl-*sn-glycero*-3-phosphocholine (POPC, ≥99% purity) and *n*-octyl-β-D-glucopyranoside (NOG, ≥98% purity) were purchased from Avanti Polar Lipids. Chloroform (Sigma Aldrich, ≥99.8% purity) served as the organic solvent for POPC. The fluorescent probes triethylammonium salt (Texas Red DHPE, ≥98% purity) and Alexa Fluor™ 488 NHS Ester (succinimidyl ester, ≥95% purity) were obtained from Invitrogen. Aquaporin 4 (≥95% purity by HPLC) was sourced from Sigma Aldrich, while salts for PBS buffer (pH = 7.4), including sodium chloride (NaCl, ≥99.5%), potassium chloride (KCl, ≥99.5%), monopotassium phosphate (KH_2PO_4, ≥99.0%), and dipotassium hydrogen phosphate (K_2HPO_4, ≥98.0%) of analytical reagent (AR) grade were purchased from SRL company. A 26G (approximately 0.45 mm outer diameter) needle of 1 mL syringe, from HMD Dispovan was used to fabricate micropores on the substrate. Aluminium sheets with a thickness of 18 μm (BBHomes company) were employed, and oxalic acid (≥99.5% purity, AR grade) from SRL company was used to prepare the electrolyte solution for the anodization process.

Substrate fabrication

Microporous aluminium substrates were fabricated by manually puncturing 18 μm thick aluminium sheets. The sheets were cleaned with a 95% ethanol solution and distilled water to remove any contaminants. A needle with a diameter of approximately 0.45 mm was positioned perpendicular to the aluminium surface and used to create the micropores. This process was repeated to generate a grid pattern of micropores across the sheet.

To create a nanoporous surface, the cleaned aluminium sheets underwent an anodization process. This involved immersing the sheets in a 0.3 M oxalic acid electrolyte solution and applying a constant 40 V voltage between the aluminium sheet (working electrode) and a platinum counter electrode using a DC power supply.[15,16] This procedure resulted in the formation of a uniform nanoporous alumina (aluminium oxide) layer on the aluminium surface (Fig. 1). Following anodization, the sheets were thoroughly rinsed with distilled water to
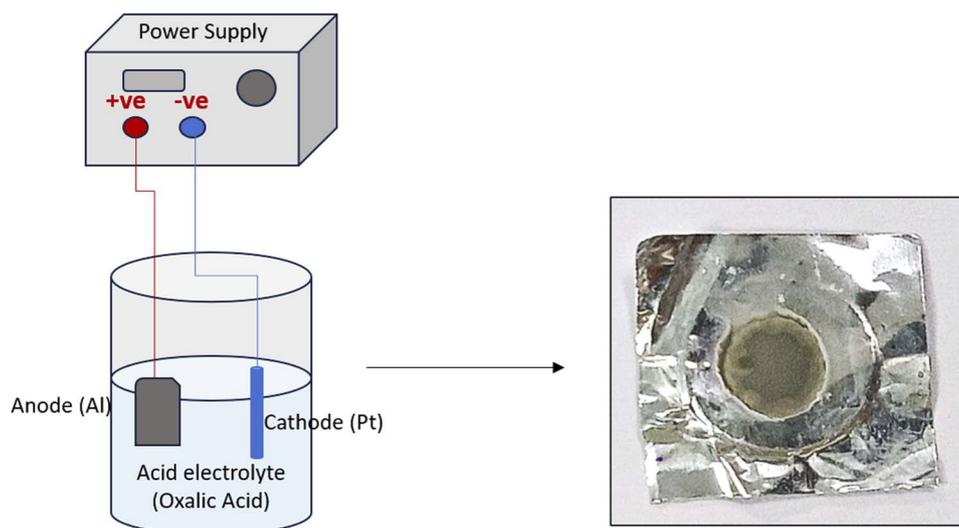

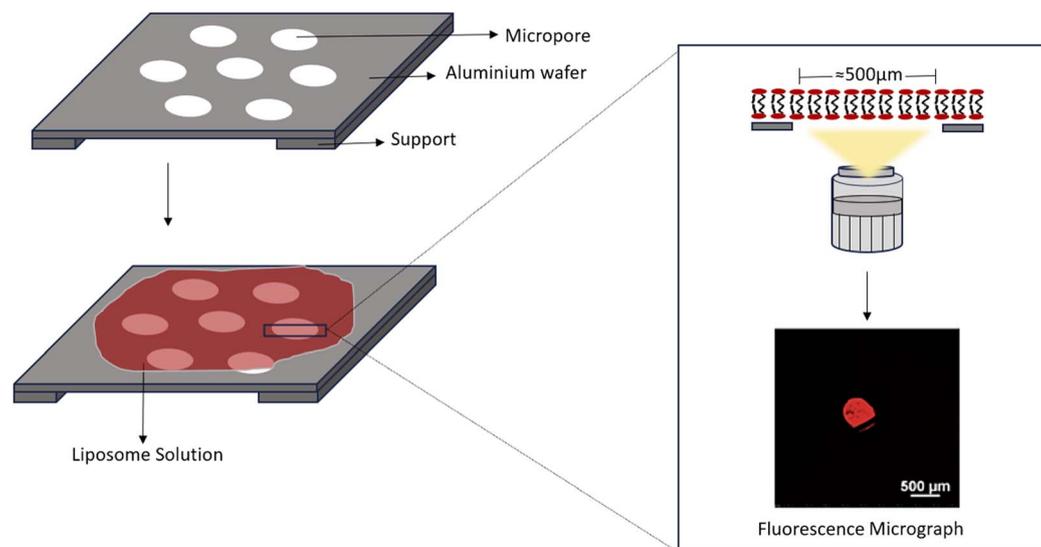Fig. 1 Anodization of aluminium sheets to develop nanopores (alumina).

Fig. 2 Schematic representing formation of the suspended lipid bilayer on the microporous substrate. The right panel shows the setup of fluorescence microscopy for DHPE Texas Red-doped lipids forming a pore-spanning lipid bilayer.

eliminate any residual oxalic acid, ensuring a clean and stable nanoporous surface for subsequent use.

Liposome and bilayer formation

Liposomes were prepared by first dissolving POPC lipid powder (2.5% w/v) in chloroform, *i.e.* a stock solution of 32.89 mM was prepared in chloroform at 25 mg mL^{-1}, and doped with Texas Red DHPE, 0.2% v/v. The chloroform was then evaporated under a stream of nitrogen gas, leaving a thin lipid film on the inner wall of a glass bottle. This film was further dried in a laminar hood for one hour to ensure complete solvent removal. PBS buffer (pH 7.4) was added to hydrate the lipid film, and the mixture was vortexed for 10 minutes to ensure thorough mixing. The final lipid molar concentration was 1.64 mM. Subsequent sonication for 30 minutes results in the formation of liposomes. To obtain homogenous liposomes, the solution was extruded (8–11 passes) through a 100 nm polycarbonate membrane using an Avanti Mini Extruder.[17–20] The extruded POPC liposome solution was carefully applied to the porous substrate, allowing the pores to be filled. This setup was incubated for 30–40 minutes at room temperature, allowing the liposomes to self-assemble into a continuous lipid bilayer across the substrate surface (Fig. 2).[12,21–23] After incubation, excess liposome solution was gently removed by washing the substrate with PBS buffer (pH 7.4). This washing step required delicate handling to prevent any disruption to the fragile lipid bilayer formed on the porous substrate. A video (Video 1) showing the formation of the suspended lipid bilayer is attached to the MS for visualization.

Microscopy and FRAP

For detailed fluorescence analysis, lipid bilayers doped with Texas Red DHPE and proteins labelled with Alexa Fluor™ 488 NHS ester (succinimidyl ester) were visualized using a Nikon Eclipse Ti2 confocal microscope. Fluorescence Recovery After Photobleaching (FRAP) experiments were conducted on the

same confocal microscope. Photobleaching was achieved using a high-intensity laser beam to bleach the Region of Interest (ROI), and recovery curves at specific time intervals were analysed to study mobility in the system.[17–19,24] The FRAP experiments are generally conducted using lipid bilayers on a solid support to monitor the mobility of individual lipid molecules. However, some previous studies have also used FRAP to evaluate diffusion in pore-spanning bilayers or suspended configurations.[25,26] We also tried to inspect the mobility of the lipid in a suspended system, where bilayers formed partially or transiently over the porous substrate.

Reconstitution of AQP protein

To achieve successful protein reconstitution within liposomes, a detailed protocol was followed, beginning with the determination of the critical micelle concentration (CMC) of the NOG detergent *via* lipid turbidity measurements, as discussed in our previous papers.[17,18] The reconstitution process involved adding 0.5376 nM AQP protein and 10.26 mM NOG detergent to the dried lipid with phosphate-buffered saline (PBS, pH 7.4) to create an aqueous solution. This mixture was vortexed for 10 minutes to ensure proper mixing and further steps for the formation of liposomes and lipid bilayers continued, as discussed in above sections. The detergent used for insertion was removed by continuous washing during bilayer formation using PBS (pH = 7.4), as established in our previous publication.[17,18]

Characterization of the AQP-reconstituted system

Proteoliposomes were analysed on the basis of changes in size and surface charge using dynamic light scattering (DLS) and zeta potential measurements using a Zeta Nano ZS (Malvern Instruments).[27] Application of proteoliposomes onto anodized nanoporous substrates was monitored using impedance spectroscopy (Autolab PGSTAT204) across a frequency range of 10 Hz to 10 kHz. A two-electrode system including a working

electrode, and a reference electrode connected to a potentiostat was used for impedance measurement.[15,16] PBS (pH = 7.4) at 1× concentration was used as the electrolyte solution for the measurement due to its physiological ionic strength and compatibility with proteoliposome systems.

Forward osmosis setup

To investigate the water transport ability of aquaporin embedded in lipid bilayers, a customized forward osmosis (FO) setup was designed.[27] This chamber utilized a 0.1 M NaCl solution as the draw solution (high-concentration solution) to generate osmotic pressure, driving water movement across the membrane. The feed solution, located on the opposite side of the membrane, consisted of deionized water (low-concentration solution). Water flow from the feed solution to the draw solution occurred due to the osmotic pressure gradient. The nanoporous substrate served as a stable support for the lipid bilayer and embedded aquaporin. To monitor water transport, Coomassie Blue dye was added to the high-concentration solution, and changes in its concentration were tracked using UV-Visible spectroscopy at 563 nm.[28] The initial absorbance of the draw solution was recorded, and as water flowed across the membrane, dilution of the draw solution led to a decrease in dye concentration and absorbance. This provided a quantitative measure of aquaporin-facilitated water transport.

All experiments were performed in triplicate ($n = 3$) unless otherwise specified. For experiments with a different number of replicates, the exact number is mentioned in the relevant figure legends or the Results section.

Results

Characterization of the suspended lipid bilayer on the microporous substrate

We investigated aluminium-based substrates of 18 μm thickness as a potential scaffold for suspended lipid bilayer formation and subsequent protein incorporation. Initially, we fabricated micropores on aluminium sheets and assessed the formation and stability of 1-palmitoyl-2-oleoyl-*glycero*-3-phosphocholine (POPC) lipid bilayers using fluorescence microscopy. Micropores of approximately 500 μm were fabricated on aluminium sheets as substrates for pore-spanning lipid bilayers. Fluorescence microscopy, employing Texas Red DHPE-doped POPC, was used to visualize bilayer formation across the micropores (Fig. 3). The observations at Day 0 showed bilayer coverage with some pores exhibiting complete and uniform fluorescence while others displayed uneven lipid deposition. A quantitative analysis of pore coverage (number of experimental repeats (n) = 5, and pores per sample (p) = 3), categorized into three distinct ranges (0–10%, 10–50%, and >50%, shown in the pie chart), indicated that a significant number of the pores exhibited greater than 50% coverage immediately after bilayer formation. However, subsequent imaging after 24 hours (Day 1) revealed a dramatic reduction in bilayer coverage. The majority of pores now fell within the 0–10% coverage range, indicating substantial bilayer disruption. This temporal instability underscores the challenges associated with maintaining

lipid bilayer integrity on microporous aluminium substrates. Various factors may contribute to this observed instability. The lipid bilayers, when supported on porous structures with high surface area, might experience weak adhesion, promoting bilayer detachment. Environmental factors and mechanical disturbances could further compromise bilayer stability.[2,11]

Furthermore, we employed fluorescence microscopy to visualize the lipid bilayer using fluorescently-labelled lipids. To study the dynamics of the lipid bilayer, we performed experiments, which allowed us to measure the mobility of the lipids within the bilayer. The FRAP experiment illustrated in the image demonstrates the lateral mobility of molecules within the lipid bilayer supported on the microporous substrate, indicating its fluid nature (Fig. 4). The microscopy images show a bleached region where fluorescence was intentionally reduced, followed by post-bleach and post-recovery stages. The graph plots the normalized fluorescence intensity over time, where key parameters such as F_0 (initial intensity), F_i (post-bleach intensity), F_∞ (final recovered intensity), $F_{1/2}$ (mid-recovery intensity), and $T_{1/2}$ (time to half recovery) are identified to calculate diffusion coefficient (D), which was 1.71 ± 0.18 μm^2 s^{-1}. The measured diffusion coefficient for the pore-spanning POPC bilayer is comparable to values previously reported for solid-supported POPC bilayers (1.66 μm^2 s^{-1}), indicating similar lipid mobility, slightly higher likely due to reduced substrate interaction.[24,29,30] This model accounts for deviations from simple exponential recovery kinetics and enables extraction of key parameters, including mobile fraction, immobile fraction, half-time of recovery, and diffusion coefficient, discussed in SI Appendix Section 1.4.

Approaches to inspect coverage and consistency of the lipid bilayer

Since, non-uniformity in pore coverage were observed during initial lipid bilayer formation, we implemented some experimental strategies aimed at optimizing the process on microporous substrates. These strategies were designed to address the challenges of incomplete or uneven bilayer deposition, as well as the subsequent temporal instability observed over a 24-hour period, as shown in Fig. 5. In Panel A, the "2× Concentration" condition, increasing the concentration of POPC twofold appears to fill micropores with suspended bilayer with initial pore coverage (Day 0) of >50% (pie chart, Fig. 3), as observed by a uniform fluorescence signal over the pores. However, by Day 1 (after 24 hours), there was a visible reduction in fluorescence intensity, indicating that the increasing lipid concentration does not prevent temporal instability of the bilayer. In the initial experiments, moving the substrate between preparation and imaging likely disturbed the bilayer and reduced its stability on micropores. In the "Stationary Substrate" condition (Panel B), the substrate was fixed on the microscope platform throughout the experiment, and images were taken at different time points over 24 hours to monitor stability. This reduced handling disturbances and allowed the system to rest overnight without external perturbation. This approach yielded some improvement in stability among the
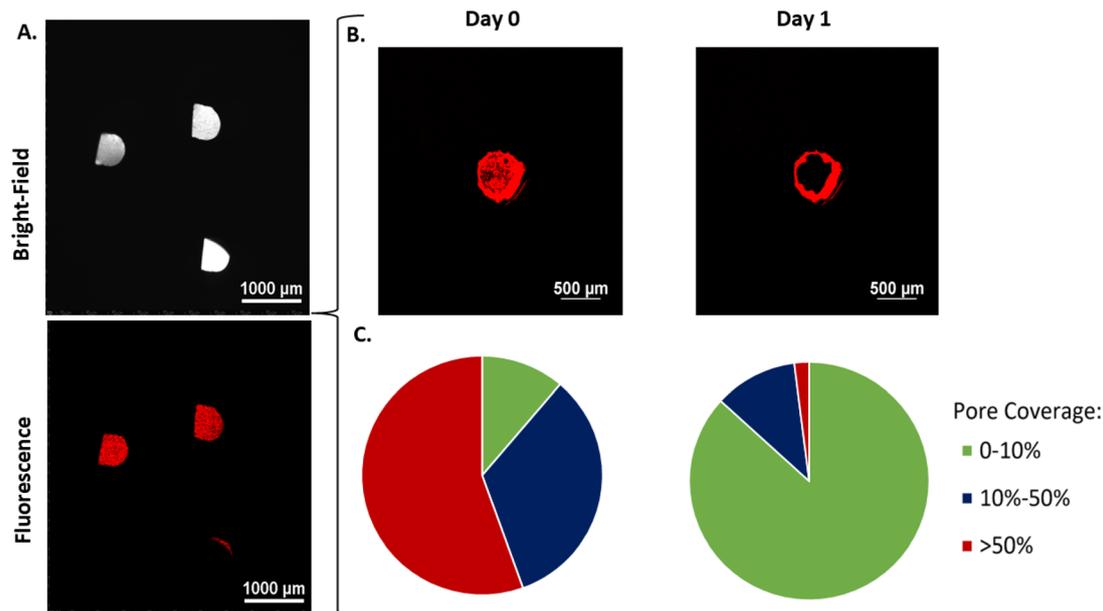
Fig. 3 Lipid bilayer formation on aluminium substrate micropores. (A) The arrangement of circular pores on an aluminium substrate, with lipid bilayers prepared over these pores. The lipids were tagged with Texas Red DHPE fluorescent dye, revealing that while some pores achieved consistent bilayer coverage, others displayed variability in deposition. (B) The pore coverage on Day 0 and after 24 hours (Day 1), showing the distribution and stability of lipid bilayer coverage over time. (C) Pie charts comparing the probability of pore coverage by the lipid bilayer on Day 0 (left) and Day 1 (right). The analysis categorizes micropore coverage into three ranges: green (0–10% coverage) indicates minimal bilayer coverage; blue (10–50% coverage) represents intermediate bilayer coverage; and red (>50% coverage) indicates pores with significant bilayer coverage, where more than 50% of the pore area is covered.
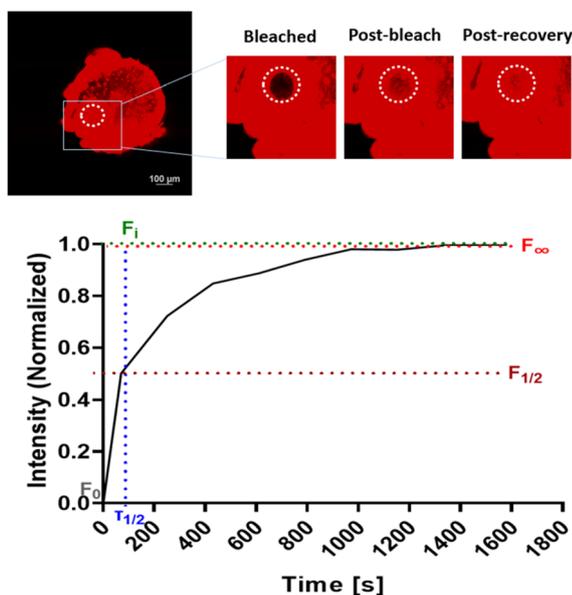

Fig. 4 Fluorescence Recovery After Photobleaching (FRAP) of the lipid bilayer suspended on the microporous substrate. In the upper panel, the insets show the ROI (region of interest) at three time points: bleached, post-bleached and post-recovery. The lower panel represents the intensity recovery curve along with different parameters used to analyse the diffusion coefficient (D) of the POPC lipid bilayer in the system.

other approaches (discussed in SI Appendix). However, it should be noted that in practical applications some degree of handling and disturbance of the system is unavoidable, and

thus the 'undisturbed/stationary substrate' condition represents an ideal arrangement than a practical application.

In another approach, "Stepwise Liposome Deposition", shown in Panel C, a liposomal solution of 1.64 mM POPC was added gradually in sequential drops (∼20 μL per drop) onto the pre-formed bilayer, with short intervals between additions, and images were captured after each step to monitor changes in pore coverage. A gradual increase in fluorescence was observed, accompanied by the formation of tunnel-like structures around the pore. This phenomenon appears to be a result of physical interactions at the pore boundaries, where repeated additions induce physical processes potentially linked to mode-optics. These effects may result from the refractive index contrast between the lipid bilayer and the surrounding substrate, coupled with curvature-induced light scattering within the porous substrate.[31,32] Thus, the stepwise liposome deposition approach introduces distinct optical effects but its impact on bilayer stability remains limited.

Shifting to nanoporous substrates

To study suspended bilayer behaviour in 1000-fold smaller pores, we employed anodization—a controlled electrochemical oxidation process—to reduce the pore size of the substrate to the nanoscale. This shift from microporous to nanoporous architecture was aimed at mitigating bilayer fragility and enhancing membrane stability by providing tighter physical support and reducing the unsupported span. This technique transforms the aluminium surface into aluminium oxide (or alumina), creating nanoporous structures. The morphological
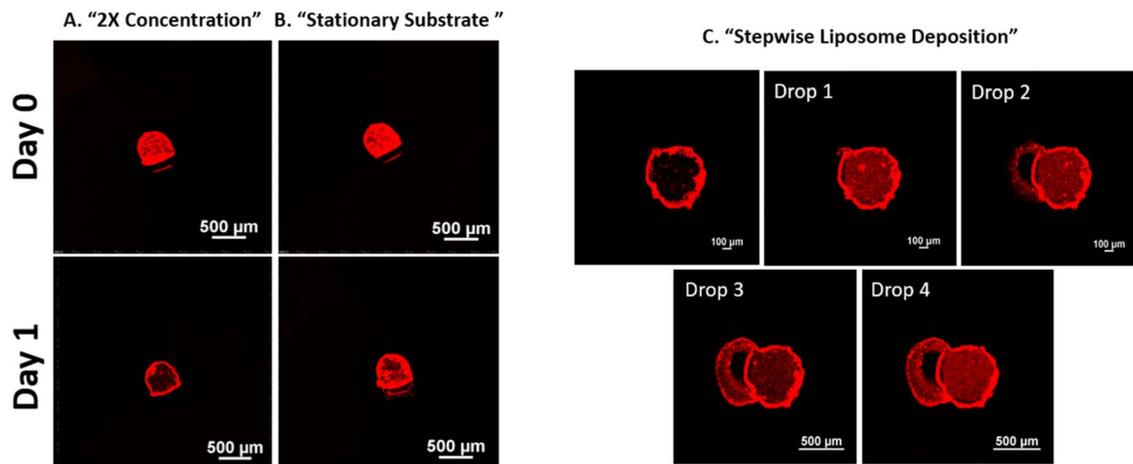
Paper

Nanoscale Advances

Fig. 5 Fluorescence microscopy observations of lipid bilayer formation and stability on microporous substrates under three experimental conditions: (A) "2× Concentration," (B) "Stationary Substrate," and (C) " Stepwise Liposome Deposition" approach.
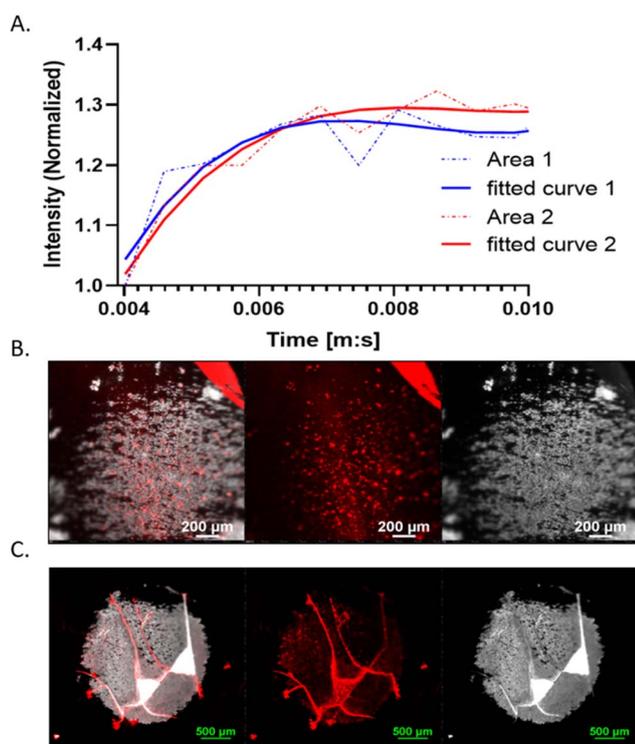

Fig. 6 Analysis of lipid bilayer formation and mobility on nanoporous anodized aluminium oxide substrates. (A) FRAP (Fluorescence Recovery After Photobleaching) results showing normalized fluorescence intensity over time in two regions (Area 1; Area 2). The blue dashed line represents the recovery curve and the blue solid line represents the fitted curve of recovery curve for Area 1. The red dashed line represents recovery curve and the red solid line represents the fitted curve of recovery curve for Area 2. (B) Microscopy images of the lipid bilayer on nanoporous substrates. (C) Images showing structural fissures in the anodized aluminium oxide substrate.

characteristics of these nanoporous membranes, including average pore diameter and interpore spacing, have been thoroughly characterized and reported in our previous work,[16]

where SEM analysis indicated the formation of irregular pores with an average diameter of 30 ± 10 nm and an interpore spacing of 40 ± 7 nm. These nanoporous substrates provide better stability for lipid bilayers due to their smaller pore size, which minimizes the chances of bilayer collapse.

Fig. 6 illustrates the analysis of lipid bilayer formation and mobility on nanoporous anodized aluminium oxide substrates, presenting both advantages and challenges in imaging and structural stability. Panel A depicts fluorescence recovery after photobleaching (FRAP) data, showing the normalized fluorescence intensity over time in two different regions (Area 1; Area 2). However, there was difficulty in defining precise regions of interest (ROIs) at the nanoscale, when using FRAP on nanoporous substrates. The x-axis represents the time of the recovery phase post-photobleaching, and the y-axis displays normalized fluorescence intensity over time.[24,29,30] In Area 1, the recovery data are represented by a blue dashed line, with a fitted curve shown as a solid blue line. Similarly, Area 2 is represented by a red dashed line and a corresponding solid red fitted curve. The recovery curves plotted with experimental data points showed an irregular and zigzag pattern, rather than the smoother recovery curves we obtained in the FRAP experiment in micropores (comparison is discussed in SI Appendix). The data were fitted using an exponential model, $Y_{fit} = A(1 - \exp(-k \times t^n))$, where A is the maximum recovery, k is the rate constant, t is time, and n is a stretching exponent (discussed in SI Appendix, Section 1.4). The fitted curves closely align with the experimental data points, indicating an eventual increase in fluorescence intensity after photobleaching. Overall, the FRAP analysis indicates active lipid mobility within the system. Panel B displays fluorescence images of the Texas Red DHPE mixed POPC lipid bilayer on the nanoporous substrate. The images reveal limited resolution in standard imaging confocal microscopy, when applied to nanoporous materials. Advanced imaging techniques like electron microscopy can easily resolve images at the nanoscale, but lack compatibility with fluorescence-based real-time analysis. Panel C represents the structural fragility of the anodized aluminium
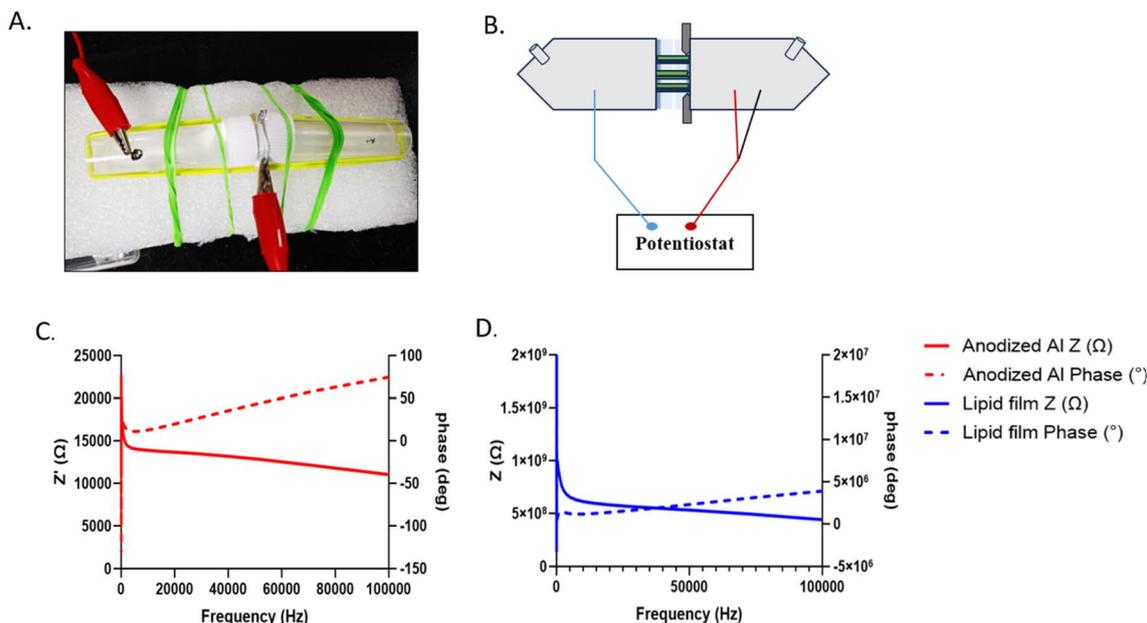
Fig. 7 (A) Physical assembly of the chamber with a securely mounted aluminium sheet. (B) Schematic of the two-electrode system: working (blue) and reference (red) electrodes connected to a potentiostat for impedance spectroscopy. Electrochemical measurements at various stages were conducted using impedance spectroscopy: (C) aluminium oxide (alumina) and (D) bilayer formation on alumina. The impedance spectroscopy data are presented, with impedance magnitude (Z') on the left y-axis and phase angle (in degrees) on the right y-axis, both plotted as functions of frequency on the x-axis.

oxide substrate. The images demonstrate significant physical damage resulting from slight disturbances.

Impedance measurement to monitor the system

To study bilayer formation on nanoporous substrates, we employed electrochemical impedance spectroscopy (EIS) as a label-free and sensitive technique to monitor membrane integrity and dynamics in real time. This method is particularly effective for suspended bilayers. It is important to note that an intact lipid bilayer forms a giga seal over the nanopores—an essential criterion indicating successful bilayer formation. The giga seal creates a high-resistance barrier that minimizes ion flow, reflected in a sharp increase in impedance, typically reaching values in the gigaohm (GΩ) range. This high impedance confirms the formation of a continuous, defect-free bilayer.[15,16] Besides, to monitor bilayer formation on nanoporous substrates, a chamber system was developed. This closed chamber system mitigates the limitations associated with the fragility and imaging challenges of nanoporous substrates, ensuring experimental comprehensive analysis of lipid bilayer dynamics. It enables multiple processes, such as anodization of aluminium sheets, lipid bilayer formation, aquaporin protein insertion, and electrochemical measurements, to occur simultaneously in a controlled environment.

In Fig. 7, Panel A shows the physical setup of the chamber, where the aluminium sheet is centrally positioned and securely fastened to maintain stability throughout the process, and Panel B provides a schematic representation of the chamber integrated with a two-electrode system used for impedance spectroscopy.[33] In this configuration, the aluminium sheet acts as the working electrode (blue), serving as the site for anodization and bilayer monitoring. The reference electrode (red) provides a stable potential for accurate voltage measurements. Additionally, the chamber is equipped with inlets and outlets for the controlled flow of reagents and solutions, allowing dynamic manipulation of experimental conditions.

Electrochemical measurements at each stage were performed using impedance spectroscopy, a technique that measures the resistance to alternating current in the system. As previously reported, the formation of an alumina layer typically results in impedance in the kilo-ohm range. In contrast, the presence of a lipid bilayer significantly increases the resistance to giga-ohm levels.[15,16] This dramatic increase is attributed to the formation of a "giga-seal," a characteristic feature of intact lipid membranes.[34,35] By exploiting this difference in impedance between the alumina substrate and the lipid bilayer, the system's properties were analysed. The impedance data are presented as a plot (Fig. 7), which displays the impedance magnitude (Z') and phase angle as functions of frequency. The plot shows how the electrical properties of the system change at each step. Initially, the bare alumina substrate had an impedance of about 15 kΩ, which aligns with the expected value reported in the literature.[16] This confirmed that the anodized alumina substrate was properly formed. However, once a lipid bilayer was prepared on the nanoporous alumina, it effectively sealed the nanopores, acting as a barrier to electron flow. This resulted in a dramatic increase in impedance to the giga-ohm range reaching up to 2 GΩ, indicating the high resistance characteristic of intact lipid membranes (the giga-seal effect).[34,35]
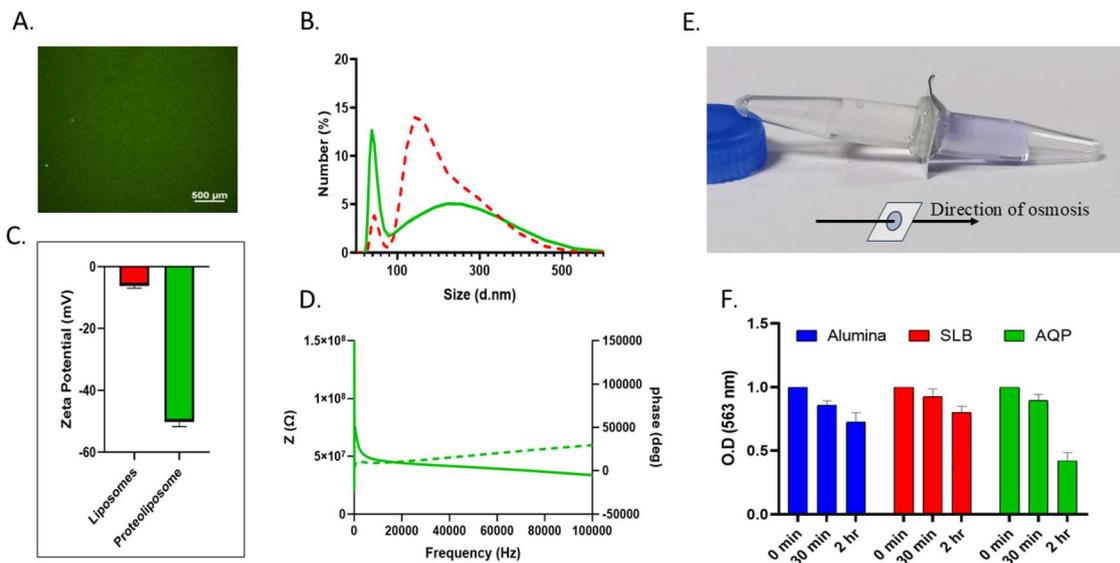
Fig. 8 (A) Fluorescence image of the AQP-inserted POPC lipid bilayer on the glass substrate. (B) DLS graphs indicating size distribution in liposome (red) and proteoliposome (green) solutions. (C) Zeta potential indicating the surface charge. (D) Impedance measurement. (E) Customized setup for checking forward osmosis. (F) OD taken at 563 nm wavelength at different time intervals: 0 min, 30 min, and 2 hours for different partition membranes, *i.e.* alumina (blue), suspended lipid bilayer (SLB, red), and aquaporin (AQP, green).

AQP insertion and its characterization

The study further investigated the efficiency of the system to study transmembrane proteins by reconstituting a water-channel membrane protein, aquaporin. Protein insertion into the POPC lipid bilayer was achieved using a detergent-mediated method established earlier,[17,18,29] and its uniform distribution within the bilayer was confirmed *via* fluorescence microscopy using Alexa Fluor 488 (Fig. 8A). DLS analysis revealed that the incorporation of aquaporin induced a notable decrease in liposome size, with the average diameter shifting from 120–180 nm for POPC liposomes to a smaller size for proteoliposomes (Fig. 8B). This size reduction is attributed to aquaporin-induced lipid bilayer compression and bending.[27] Furthermore, zeta potential measurements suggest a shift from a near-neutral surface charge for POPC liposomes to a strongly negative value exceeding −40 mV for proteoliposomes (Fig. 8C). This change reflects the influence of negatively charged aquaporin on the liposome surface charge and the formation of an electrical double layer, contributing to enhanced proteoliposome stability.[29] The insertion of aquaporin into the lipid bilayer led to a decrease in bilayer impedance from giga-ohm to mega-ohm range, stabilizing around 5 MΩ (Fig. 8D), due to the opening of channels in the bilayer system.

To assess aquaporin's water transport efficiency, a customized forward osmosis (FO) setup was fabricated (Fig. 8E).[27] The setup included 0.1 M NaCl draw solution and deionized water feed solution, separated by a nanoporous substrate. Water transport across the membrane was monitored by measuring changes in the absorbance of Coomassie blue dye added to the draw solution at 563 nm using UV-Visible spectroscopy. Forward osmosis experiments were conducted under three conditions: bare alumina, suspended lipid bilayer (SLB), and

aquaporin-embedded SLB (AQP-SLB). The AQP-SLB system exhibited the most efficient water transport, as evidenced by a significant decrease in absorbance over time (Fig. 8F). The bar graph in Fig. 8F illustrates the optical density (O.D.) at 563 nm for three systems—alumina, supported lipid bilayer (SLB), and aquaporin-based membrane (AQP)—measured at 0 minutes, 30 minutes, and 2 hours. The alumina system (blue bars) shows a gradual reduction by 2 hours. The SLB system (red bars) maintains its O.D. at 0 and 30 minutes, with only a slight decrease by 2 hours. In contrast, the AQP system (green bars) exhibits a sharp drop by 30 minutes and a further decline at 2 hours, reaching nearly half of the initial value.

Discussion

This study systematically explores the critical role of micro- and nanoporous substrates in forming and stabilizing suspended lipid bilayers, while also investigating the functional incorporation of aquaporin. The findings underscore significant differences in the behaviour and stability of lipid bilayers supported on microporous *versus* nanoporous substrates, elucidating the interplay between pore geometry and bilayer dynamics.

Microporous substrates and challenges

We used fluorescence microscopy with fluorescently-labelled lipids to visualize the lipid bilayer and study its dynamics. Fluorescence microscopy revealed partial coverage of the micropores by lipid bilayers, with more than 50% of the pores demonstrating significant bilayer formation immediately after assembly. However, the temporal instability observed, characterized by substantial disruption and loss of bilayer integrity

within 24 hours, underscores the limitations of microporous substrates for long-term studies (Fig. 3). Factors such as weak adhesion, environmental disturbances, and the mechanical fragility of the lipid bilayer likely contributed to this instability. Furthermore, FRAP experiments were performed to measure the lateral mobility of lipids within the bilayer supported on a microporous substrate. Microscopy images captured the bleached region, post-bleach, and post-recovery stages, while the corresponding graph showed normalized fluorescence intensity over time (Fig. 4). The measured diffusion coefficient was $1.71 \pm 0.18 \ \mu m^2 \ s^{-1}$, confirming the bilayer's dynamic behaviour. In previous studies, POPC bilayers on solid substrate showed a diffusion coefficient of $1.66 \ \mu m^2 \ s^{-1}$, which decreased to $1.14 \ \mu m^2 \ s^{-1}$ upon the addition of other lipid components (cholesterol and sphingomyelin).[24] Camley *et al.* analysed diffusion in free *vs.* supported membranes. They showed that the presence of a solid support alters the hydrodynamic boundary conditions and generally slows diffusion compared to a "free" membrane environment. Whereas suspended bilayers have advantages of reduced substrate interactions. This implies that suspended bilayers may better preserve the intrinsic mobility of lipids (*i.e.* less damping by the substrate) compared to supported ones.[9,36]

Efforts to mitigate these challenges included strategies such as increased lipid concentration, maintaining stationary substrate conditions, and stepwise liposome deposition (Fig. 5). While these methods showed modest improvements in bilayer stability, they were insufficient to overcome the fundamental instability associated with the large pore size and structural fragility of microporous substrates.

Nanoporous substrates to enhance stability

The transition to nanoporous anodized aluminium oxide substrates provided a more stable platform for lipid bilayer formation. The smaller pore size and compact arrangement of nanopores minimized the likelihood of bilayer collapse, offering improved mechanical stability. Despite these advantages, challenges in imaging nanoporous substrates were noted. The limited resolution of fluorescence microscopy at the nanoscale necessitates advanced imaging techniques, such as electron microscopy, which lack real-time compatibility. Additionally, the structural fragility of anodized substrates underlined the need for controlled experimental conditions to preserve the integrity of the nanopores (Fig. 6).

Hence, the system was preserved in a closed chamber, where each step was monitored *via* electrochemical measurements. Impedance spectroscopy confirmed the successful formation of intact lipid bilayers, characterized by a giga-seal effect with resistance reaching up to 2 GΩ (Fig. 7).[34,35]

Aquaporin incorporation and functional validation

The successful reconstitution of aquaporin into the lipid bilayers was a pivotal achievement. Dynamic Light Scattering (DLS) and zeta potential measurements revealed significant changes in liposome size and surface charge upon aquaporin incorporation, indicating the structural and electrostatic effects of the protein (Fig. 8). The reduction in impedance from the giga-ohm to the mega-ohm range further validated the functional integration of aquaporin, as the protein channels facilitated ionic transport.[37,38]

The forward osmosis experiments provided compelling evidence of aquaporin's functionality. The aquaporin-embedded suspended lipid bilayers demonstrated superior water transport efficiency compared to control systems, as evidenced by a marked decrease in dye absorbance over time. This underscores the potential of aquaporin-based membranes for applications in water purification and biomimetic systems.

The findings highlight the trade-offs between the ease of fabrication and stability in microporous substrates *versus* the enhanced stability and functional capabilities of nanoporous systems.[11,15,16] The successful reconstitution and functionality of aquaporin in these systems not only validate the approach but also demonstrate their potential for practical applications in biomimetic technologies and water purification. By addressing the identified challenges, these findings can serve as a foundation for advancing the design and utilization of porous substrates in membrane protein research and other biotechnological applications.[39,40]

Future work may explore the use of copolymers or hybrid lipid–polymer systems to improve the stability of suspended bilayers, especially on fragile nanoporous substrates. Incorporating such materials could help resist mechanical stress and extend bilayer lifetime.[41,42] Further improvements might also include refining the chamber setup for better imaging and easier membrane assembly, as well as testing other membrane proteins to expand potential applications.

Author contributions

Akanksha Kumari: writing – draft, methodology, formal analysis. Jaydeep Bhattacharya: supervision, resources, concept. Ranjita Ghosh Moulick: writing – review & editing, supervision, funding acquisition, conceptualization.

Conflicts of interest

The authors declare that they have no known competing financial interests or personal relationships that could have appeared to influence the work reported in this paper.

Data availability

All data generated or analysed during this study are included in this published article [and its supplementary information (SI) files]. Supplementary information: (SI Appendix) and Video (Video 1). See DOI: https://doi.org/10.1039/d6na00018e.

Acknowledgements

References

1 G. Fragneto, Neutrons and model membranes, *Eur. Phys. J. Spec. Top.*, 2012, **213**(1), 327–342.

2 J. Sarkis and V. Vié, Biomimetic models to investigate membrane biophysics affecting lipid–protein interaction, *Front. Bioeng. Biotechnol.*, 2020, **8**, 270.

3 R. D. Barker, L. E. McKinley and S. Titmuss, Neutron reflectivity as a tool for physics-based studies of model bacterial membranes, in *Biophysics of Infection. Advances in Experimental Medicine and Biology*, Leake M., Cham, Springer, 2016, pp. 261–282.

4 E. T. Castellana and P. S. Cremer, Solid supported lipid bilayers: from biophysical studies to sensor design, *Surf. Sci. Rep.*, 2006, **61**(10), 429–444.

5 J. Chalmeau, N. Monina, J. Shin, C. Vieu and V. Noireaux, α-Hemolysin pore formation into a supported phospholipid bilayer using cell-free expression, *Biochim. Biophys. Acta Biomembr.*, 2011, **1808**(1), 271–278.

6 C. Peetla, A. Stine and V. Labhasetwar, Biophysical interactions with model lipid membranes: applications in drug discovery and drug delivery, *Mol. Pharm.*, 2009, **6**(5), 1264–1276.

7 Y. Gerelli, Phase transitions in a single supported phospholipid bilayer: real-time determination by neutron reflectometry, *Phys. Rev. Lett.*, 2019, **122**(24), 248101.

8 M. Ahumada, E. Jacques, C. Calderon and F. Martínez-Gómez, Porosity in biomaterials: a key factor in the development of applied materials in biomedicine, in *Handbook of Ecomaterials*, Cham, Springer, 2019, pp. 3503–3522.

9 S. Ramakrishnan and J. S. Weerakkody, Suspended lipid bilayer: a versatile platform for next-gen drug discovery and biomedical applications, *Acc. Mater. Res.*, 2022, **3**(10), 996–998.

10 I. Kusters, A. M. van Oijen and A. J. Driessen, Membrane-on-a-chip: microstructured silicon/silicon-dioxide chips for high-throughput screening of membrane transport and viral membrane fusion, *ACS Nano*, 2014, **8**(4), 3380–3392.

11 A. Simon, A. Girard-Egrot, F. Sauter, C. Pudda, N. P. d'Hahan, L. Blum, *et al.*, Formation and stability of a suspended biomimetic lipid bilayer on silicon submicrometer-sized pores, *J. Colloid Interface Sci.*, 2007, **308**(2), 337–343.

12 S. E. Ayscough, L. A. Clifton, M. W. Skoda and S. Titmuss, Suspended phospholipid bilayers: a new biological membrane mimetic, *J. Colloid Interface Sci.*, 2023, **633**, 1002–1011.

13 A. Studer, X. Han, F. K. Winkler and L. X. Tiefenauer, Formation of individual protein channels in lipid bilayers suspended in nanopores, *Colloids Surf., B*, 2009, **73**(2), 325–331.

14 I. Vlassiouk, A. Krasnoslobodtsev, S. Smirnov and M. Germann, Direct detection and separation of DNA using nanoporous alumina filters, *Langmuir*, 2004, **20**(23), 9913–9915.

15 J. Drexler and C. Steinem, Pore-suspending lipid bilayers on porous alumina investigated by electrical impedance spectroscopy, *J. Phys. Chem. B*, 2003, **107**(40), 11245–11254.

16 J. Bhattacharya, A. Kisner, A. Offenhäusser and B. Wolfrum, Microfluidic anodization of aluminum films for the fabrication of nanoporous lipid bilayer support structures, *Beilstein J. Nanotechnol.*, 2011, **2**(1), 104–109.

17 M. R. Ghosh, D. Afanasenkau, S. E. Choi, J. Albers, W. Lange, V. Maybeck, *et al.*, Reconstitution of fusion proteins in supported lipid bilayers for the study of cell surface receptor–ligand interactions in cell–cell contact, *Langmuir*, 2016, **32**(14), 3462–3469.

18 A. Kumari, D. Saha, J. Bhattacharya, V. K. Aswal and R. G. Moulick, Studying the structural organization of non-membranous protein hemoglobin in a lipid environment after reconstitution, *Int. J. Biol. Macromol.*, 2023, **243**, 125212.

19 R. G. Moulick, G. Panaitov, S. E. Choi, D. Mayer and A. Offenhäusser, Patterning artificial lipid bilayer on nanostructured surfaces, *Int. J. Nanomed.*, 2018, **13**(1), 55–58.

20 R. G. Moulick, G. Panaitov, L. Du, D. Mayer and A. Offenhäusser, Neuronal adhesion and growth on nanopatterned EA5-POPC synthetic membranes, *Nanoscale*, 2018, **10**(11), 5295–5301.

21 P. Sondhi, D. Lingden and K. J. Stine, Structure, formation, and biological interactions of supported lipid bilayers incorporating lipopolysaccharide, *Coatings*, 2020, **10**(10), 981.

22 K. Kolahdouzan, J. A. Jackman, B. K. Yoon, M. C. Kim, M. S. Johal and N. J. Cho, Optimizing the formation of supported lipid bilayers from bicellar mixtures, *Langmuir*, 2017, **33**(20), 5052–5064.

23 L. Socrier and C. Steinem, Pore-spanning membranes as a tool to investigate lateral lipid membrane heterogeneity, in *Methods in Enzymology*, Academic Press, 2024, vol. 700, pp. 455–483.

24 A. Kumari, S. Kumar, V. K. Aswal, J. Bhattacharya, S. Sen and M. R. Ghosh, Protein–lipid interactions in a three-component POPC–cholesterol–sphingomyelin modulated membrane, *J. Phys. Chem. B*, 2025, **129**(40), 10298–10310.

25 M. Claesson, R. Frost, S. Svedhem and M. Andersson, Pore spanning lipid bilayers on mesoporous silica having varying pore size, *Langmuir*, 2011, **27**(14), 8974–8982.

26 A. Sannigrahi, V. H. Rai, M. V. Chalil, D. Chakraborty, S. K. Meher and R. Roy, A versatile suspended lipid membrane system for probing membrane remodeling and disruption, *Membranes*, 2022, **12**(12), 1190.

27 A. Fuwad, H. Ryu, E. D. Han, J. H. Lee, N. Malmstadt, Y. R. Kim, *et al.*, Highly permeable and shelf-stable aquaporin biomimetic membrane based on an anodic aluminum oxide substrate, *npj Clean Water*, 2024, **7**(1), 11.

28 Merck Millipore, *Coomassie Brilliant Blue R-250 (C.I. 42660), CAS 6104-59-2*, Sigma-Aldrich, [Internet], [cited 2025 Jan 27]. available from: https://www.sigmaaldrich.com/IN/en/product/mm/112553.

29 D. Afanasenkau, *Supported Lipid Bilayer as a Biomimetic Platform for Neuronal Cell Culture [dissertation]*, Forschungszentrum Jülich, 2013.

30 M. Kang, C. A. Day, A. K. Kenworthy and E. DiBenedetto, Simplified equation to extract diffusion coefficients from confocal FRAP data, *Traffic*, 2012, **13**(12), 1589–1600.

31 J. Wang and J. Dong, Optical waveguides and integrated optical devices for medical diagnosis, health monitoring and light therapies, *Sensors*, 2020, **20**(14), 3981.

32 S. D. Gupta, N. Ghosh and A. Banerjee, *Wave Optics: Basic Concepts and Contemporary Trends*, Boca Raton, CRC Press, 2015.

33 E. K. Schmitt, M. Vrouenraets and C. Steinem, Channel activity of OmpF monitored in nano-BLMs, *Biophys. J.*, 2006, **91**(6), 2163–2171.

34 K. Sugihara, J. Vörös and T. Zambelli, A gigaseal obtained with a self-assembled long-lifetime lipid bilayer on a single polyelectrolyte multilayer-filled nanopore, *ACS Nano*, 2010, **4**(9), 5047–5054.

35 S. Kresák, T. Hianik and R. L. Naumann, Giga-seal solvent-free bilayer lipid membranes: from single nanopores to nanopore arrays, *Soft Matter*, 2009, **5**(20), 4021–4032.

36 B. A. Camley and F. L. Brown, Diffusion of complex objects embedded in free and supported lipid bilayer membranes: role of shape anisotropy and leaflet structure, *Soft Matter*, 2013, **9**(19), 4767–4779.

37 C. Steinem, A. Janshoff, W. P. Ulrich, M. Sieber and H. J. Galla, Impedance analysis of supported lipid bilayer membranes: a scrutiny of different preparation techniques, *Biochim. Biophys. Acta Biomembr.*, 1996, **1279**(2), 169–180.

38 A. Puiggalí-Jou, J. Pawlowski, L. J. Del Valle, C. Michaux, E. A. Perpète, S. Sek and C. Aleman, Properties of Omp2a-based supported lipid bilayers: comparison with polymeric bioinspired membranes, *ACS Omega*, 2018, **3**(8), 9003–9019.

39 N. Teske, J. Sibold, J. Schumacher, N. K. Teiwes, M. Gleisner, I. Mey and C. Steinem, Continuous pore-spanning lipid bilayers on silicon oxide-coated porous substrates, *Langmuir*, 2017, **33**(49), 14175–14183.

40 D. Tadaki, D. Yamaura, S. Araki, M. Yoshida, K. Arata, T. Ohori, *et al.*, Mechanically stable solvent-free lipid bilayers in nano- and micro-tapered apertures for reconstitution of cell-free synthesized hERG channels, *Sci. Rep.*, 2017, **7**(1), 17736.

41 G. Bello, F. Cavallini, L. A. Dailey and E. K. Ehmoser, Supported polymer/lipid hybrid bilayers formation resembles a lipid-like dynamic by reducing the molecular weight of the polymer, *Biochim. Biophys. Acta Biomembr.*, 2021, **1863**(1), 183472.

42 E. Brodszkij and B. Städler, Advances in block copolymer–phospholipid hybrid vesicles: from physical–chemical properties to applications, *Chem. Sci.*, 2024, **15**(28), 10724–10744.